

# Slow decay processes of electrostatically trapped Rydberg NO molecules

A. Deller,\* M. H. Rayment, and S. D. Hogan

*Department of Physics and Astronomy, University College London,  
Gower Street, London WC1E 6BT, United Kingdom*

(Dated: February 9, 2022)

Nitric oxide (NO) molecules initially traveling at 795 m/s in pulsed supersonic beams have been photoexcited to long-lived hydrogenic Rydberg-Stark states, decelerated and electrostatically trapped in a cryogenically cooled, chip-based transmission-line Rydberg-Stark decelerator. The decelerated and trapped molecules were detected *in situ* by pulsed electric field ionization. The operation of the decelerator was validated by comparison of the experimental data with the results of numerical calculations of particle trajectories. Studies of the decay of the trapped molecules on timescales up to 1 ms provide new insights into the lifetimes of, and effects of blackbody radiation on, Rydberg states of NO.

Molecules in high Rydberg states play important roles in tests of fundamental physics through measurements of ionization and dissociation energies [1]. Their decay dynamics affect recombination in atmospheric and astrophysical plasmas [2, 3], while in the laboratory they have been exploited in studies of ultracold plasmas [4, 5]. Samples in these states are also of interest for low-energy inelastic scattering including, e.g., studies of long-range dipole-dipole interactions that lead to resonant energy transfer [6–8], low-energy electron scattering that can allow the stabilization of weakly bound long-range Rydberg molecules [9, 10] and result in electron transfer [11, 12], and short-range ion-molecule reactions [13]. In these areas, advances are expected if the molecules are prepared in slowly moving, velocity-controlled beams or in traps. This would enhance resolution in spectroscopy and scattering experiments and facilitate direct measurements of lifetimes and decay dynamics over previously inaccessible timescales.

Experimental methods – including, e.g., buffer gas cooling [14], multistage Stark [15, 16] and Zeeman [17, 18] deceleration, and laser cooling [19, 20] developed for the direct preparation of cold ground-state molecules offer opportunities for studies involving high Rydberg states [21]. However, the most widely applicable approach to preparing cold, trapped Rydberg molecules involves exploiting the forces that can be exerted on them using inhomogeneous electric fields through the methods of Rydberg-Stark deceleration [22–24]. This was first implemented for beams of Kr [25] and H<sub>2</sub> [26]. Subsequent developments [27, 28] led to the realization of guides [29–33], velocity selectors [34], lenses [35], mirrors [36, 37], beam splitters [38], accelerators and decelerators [39–41], and traps [40, 42–45]. These have been demonstrated for positronium, H, D, He, Ar, Kr or H<sub>2</sub>. However, the ubiquity of Rydberg states in almost all atoms and molecules suggests that Rydberg-Stark deceleration can be extended to the preparation of cold samples of heavier and more complex species, provided they can be prepared in hydrogenic Rydberg-Stark states with static electric dipole moments  $\gtrsim 1000$  D, and lifetimes  $\gtrsim 10$   $\mu$ s.

The methods of Rydberg-Stark deceleration have allowed investigations of excited-state decay processes, including effects of blackbody radiation in H, D, He and H<sub>2</sub> on timescales  $> 1$  ms [46–50]. They have contributed to developments in positronium physics directed toward precision tests of bound-state quantum electrodynamics and antimatter gravity [51]. And they have enabled studies of the  $\text{H}_2^+ + \text{H}_2 \rightarrow \text{H}_3^+ + \text{H}$  reaction at temperatures as low as 300 mK, where contributions from individual angular momentum partial waves were identified [13]. For atoms in coherent superpositions of Rydberg states the methods of Rydberg-Stark deceleration have permitted the observation of matter-wave interference for particles with dimensions of  $\sim 300$  nm and electric dipole moments of  $\sim 11\,000$  D [52].

Here, by preparing long-lived hydrogenic Rydberg states, for which predissociation is not the dominant decay mechanism, by two-color two-photon excitation from the  $\text{X } ^2\Pi_{1/2}$  ground state [53–56], we report Rydberg-Stark deceleration and electrostatic trapping of NO. NO is a chemically important radical that plays a role in atmospheric physics, combustion and trace gas detection [57]. Measurements of the decay of the trapped molecules in environments maintained at  $T_{\text{env}} = 295$  and 30 K, and after initial excitation to states with principal quantum numbers ranging from  $n = 38$  to 44, provide new insights into the lifetimes and slow decay processes of Rydberg states of NO.

The apparatus used in the experiments is depicted in Figure. 1(a). NO molecules in pulsed supersonic beams (mean longitudinal speed  $\bar{v}_z = 810$  m/s; 25 Hz repetition rate) were photoexcited to high Rydberg states using the resonance-enhanced  $\text{X } ^2\Pi_{1/2}(v'' = 0, N'' = 1, J'' = 3/2) \rightarrow \text{A } ^2\Sigma^+(v' = 0, N' = 0, J' = 1/2) \rightarrow n\ell \text{X } ^+ ^1\Sigma^+(v^+ = 0, N^+)$  two-color two-photon excitation scheme driven by radiation from two pulsed dye lasers (FWHM spectral width  $0.17 \text{ cm}^{-1}$ ) [53–56]. The first,  $\text{P}_{11}(3/2)$ , transition occurred at  $\nu_1 = 44\,193.988 \text{ cm}^{-1}$ . Transitions from the  $\text{A } ^2\Sigma^+$  state to Rydberg states with  $n\ell(N^+) = np(0)$  and  $nf(2)$  character, where  $34 \leq n \lesssim 60$ , occurred for  $\nu_2 = 30\,435 - 30\,505 \text{ cm}^{-1}$ . Intramolecular

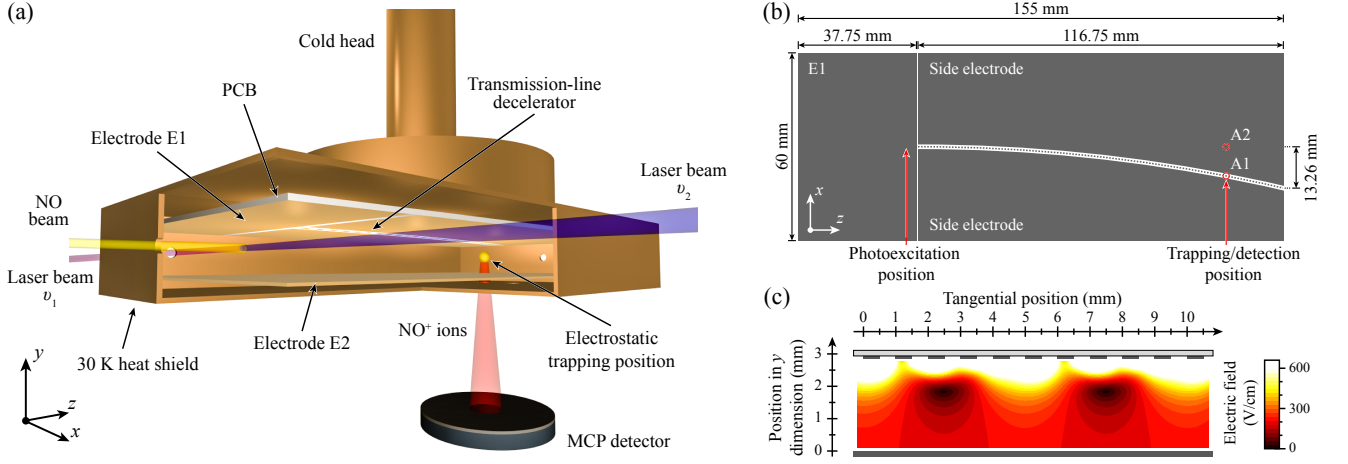


FIG. 1. (a) Schematic diagram of the apparatus (not to scale). Note: Part of the 30 K heat shield has been omitted for clarity. (b) Scale diagram of the PCB in (a) with silver-coated copper regions (insulating gaps) indicated in grey (white). The positions of detection apertures A1 and A2 in E2 are indicated by the red circles. (c) Typical electric field distribution on the axis of the decelerator in the plane perpendicular to the PCB surface for  $V_0 = 125$  V.

interactions and stray electric fields caused  $\sim 1\%$  of the excited molecules to evolve, close to the time of excitation, into long-lived  $\ell$ -mixed hydrogenic Rydberg-Stark states with  $|m_\ell| \gtrsim 3$  and static electric dipole moments between 0 and  $\sim 10\,000$  D [56].

Photoexcitation was performed beneath electrode E1, an electrically isolated  $37.75\text{ mm} \times 60\text{ mm}$  silver-coated copper region on the printed circuit board (PCB) in Figures 1(a) and (b). E1 was separated in the  $z$  dimension by a  $0.5\text{ mm}$  insulating gap from a chip-based transmission-line Rydberg-Stark decelerator [41]. This comprised a curved array of  $0.5 \times 0.5\text{ mm}$  silver-coated copper electrodes ( $1\text{ mm}$  center-to-center spacing,  $518.5\text{ mm}$  radius of curvature) on an Arlon substrate. These were separated in the  $x$  dimension from side electrodes by  $0.5\text{ mm}$  insulating gaps. The PCB was positioned parallel to, and  $3\text{ mm}$  above, the plane copper electrode E2 [see Figure 1(a)]. The decelerator and a surrounding copper heat shield were thermally coupled to a cold head operated at  $T_{\text{env}} = 295$  or  $30\text{ K}$ .

After excitation, the molecules traveled for  $5.4\text{ }\mu\text{s}$  ( $\sim 4\text{ mm}$ ) in the  $z$  dimension before the decelerator was activated (rise time  $4\text{ }\mu\text{s}$ ). At this time those in low-field-seeking (LFS) Rydberg-Stark states with positive Stark shifts were loaded into the first traveling electric trap. The decelerator was operated using five sinusoidally oscillating electric potentials (amplitude  $V_0 = 125\text{ V}$ ; frequency  $f_{\text{osc}} = v/L \leq 160\text{ kHz}$ , with  $L = 5\text{ mm}$  the spatial periodicity along the decelerator axis) applied to the electrode array in a sequence repeated every sixth electrode, and a potential  $-V_0/2$  applied to E2. A typical electric field distribution in the  $yz$  plane on the axis of the decelerator is shown in Figure 1(c). To decelerate molecules confined within the traveling traps,  $f_{\text{osc}}$  was

reduced toward zero. For  $f_{\text{osc}} = 0$  the traps remained stationary. The curvature of the decelerator minimized collisions with the trailing components of the molecular beam [46].

Detection was performed *in situ* by pulsed electric field ionization (PFI) [45]. This was implemented by switching off the decelerator and applying potentials of  $+500\text{ V}$  to the side electrodes. NO<sup>+</sup> ions generated above A1, a  $2\text{-mm}$ -diameter aperture in E2 at the position of the 101<sup>st</sup> decelerator electrode, by PFI were accelerated out from the cryogenic region to a microchannel plate (MCP) detector [see Figure 1(a)]. To allow detection by PFI when the decelerator was off, a second  $2\text{-mm}$ -diameter aperture A2 was included in E2 on the molecular-beam axis [see Figure 1(b)].

To characterize the decelerator it was cooled to  $T_{\text{env}} = 30\text{ K}$  and Rydberg states with  $43f(2)$  character were excited. This led to the population of long-lived hydrogenic Rydberg-Stark states with  $n = 43$  and  $N^+ = 2$  that had static electric dipole moments between 0 and  $6400\text{ D}$ . Time-of-flight (TOF) measurements between the photoexcitation and detection positions ( $105\text{ mm}$ ) were then made. A reference measurement performed with the decelerator off is displayed as the black curve in Figure 2. From the  $\sim 130\text{ }\mu\text{s}$  mean measured flight time, a mean longitudinal speed of  $\bar{v}_z = 810\text{ m/s}$  was determined. The decelerator was then activated to transport molecules in LFS Rydberg-Stark states to the detection position above A1 at a constant speed of  $795\text{ m/s}$ , i.e., the tangential acceleration was set to  $a_t = 0\text{ m/s}^2$ . The resulting TOF distribution (red curve in Figure 2) exhibited a larger amplitude and smaller FWHM than that recorded with the decelerator off. These arose because of the reduced velocity dispersion of the molecules when

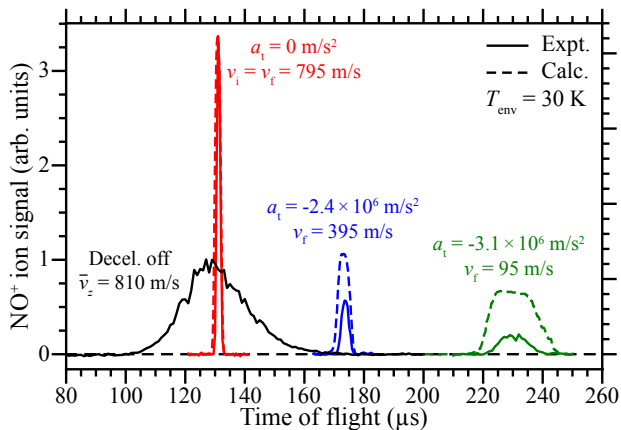


FIG. 2. Experimentally recorded (continuous curves) and calculated (dashed curves) TOF distributions for Rydberg NO molecules from their position of photoexcitation to the detection position on the molecular beam axis with the decelerator off (black curve), and above aperture A1 for  $a_t = 0$ ,  $-2.4 \times 10^6$  and  $-3.1 \times 10^6$  m/s<sup>2</sup> as indicated.

transported in the traveling traps.

The molecules were decelerated from 795 to 395 m/s (95 m/s) by chirping the frequency of the oscillating potentials [45] such that  $a_t = -2.4 \times 10^6$  m/s<sup>2</sup> ( $a_t = -3.1 \times 10^6$  m/s<sup>2</sup>) as seen from the continuous blue (green) curve in Figure 2. The measured arrival times at the detection position are in good quantitative agreement with the results of numerical calculations of particle trajectories (dashed curves). In these calculations the initial phase-space distribution of 10 000 molecules was defined from the measured dimensions of the laser beams, geometry of the apparatus, and TOF distributions recorded with the decelerator off. The distribution of Rydberg-Stark states with  $n = 43$  was described by a Gaussian function centered on the Stark state with zero static electric dipole moment as determined from the electric field ionization measurements reported in Ref. [56]. The reduction in the amplitude of the TOF signal as  $|a_t|$  was increased is a consequence of the reduced phase-space acceptance under these conditions and the geometry of the *in situ* detection region [41]. The discrepancies between the amplitudes of the measured and calculated TOF distributions arise from the finite decay time of the Rydberg states, which was not accounted for in the calculations. The lifetimes of the Rydberg states are influenced by spontaneous emission, intramolecular interactions, transitions induced by blackbody radiation, and the electric fields in the traveling traps. To study these processes in a controlled way it is necessary to bring the traps to rest in the laboratory-fixed frame of reference.

Electrostatic trapping was achieved by setting  $a_t = -3.15 \times 10^6$  m/s<sup>2</sup> so that the trap in which the molecules were transported was stopped above A1. When station-

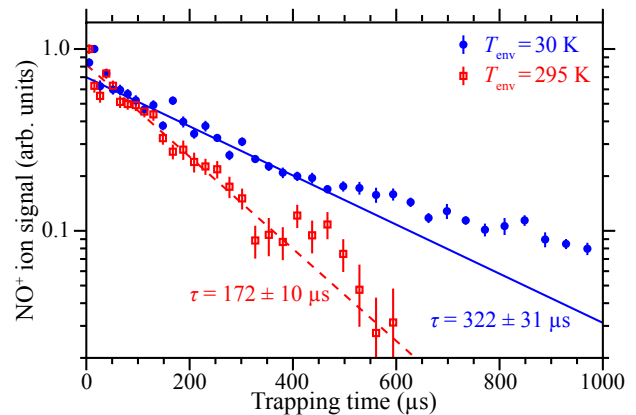


FIG. 3. Decay of electrostatically trapped Rydberg NO molecules initially excited to states with  $n = 43$  and  $N^+ = 2$  for  $T_{\text{env}} = 30$  and 295 K, as indicated. The continuous (dashed) curves represent single exponential functions fit to the data for trapping times between 50 and 350  $\mu\text{s}$  (see text for details).

ary, changes in the PFI signal over time reflected motion in, and decay from, the trap. The results of trap-decay measurements performed with molecules prepared in states with  $n = 43$  and  $N^+ = 2$  are displayed in Figure 3. Data recorded for  $T_{\text{env}} = 30$  K (295 K) are indicated by the filled circles (open squares). The origin of the horizontal axis represents the time at which the traps stopped moving. For both measurements, equilibration of the motion of the molecules that occurred after the traps were stopped contributed, in part, to the changes observed in the NO<sup>+</sup> signal at trapping times  $t_{\text{trap}} \lesssim 50$   $\mu\text{s}$ .

For  $T_{\text{env}} = 30$  K, 10 – 100 molecules were trapped at a density of  $\sim 10^4$  cm<sup>-3</sup> in each experimental cycle. With  $V_0 = 125$  V, the translational temperature of the trapped molecules, measured by monitoring their rate of dispersion after switching off the trapping fields, was  $E_{\text{kin}}/k_B = 20.5 \pm 0.8$  K, the trap depth for the outermost  $n = 43$ ,  $|m_\ell| = 3$  Rydberg-Stark states was  $E_{\text{trap}}/k_B \simeq 30$  K, and, as seen in Figure 3 two main decay components were observed for  $t_{\text{trap}} \geq 50$   $\mu\text{s}$ . These are reminiscent of the decay of H Rydberg atoms from cryogenic electrostatic traps [46, 49]. The faster component is described by a single exponential function with a time constant of  $\tau = 322 \pm 31$   $\mu\text{s}$  (continuous blue curve) for  $50 \leq t_{\text{trap}} \leq 350$   $\mu\text{s}$ , and attributed primarily to the decay of the  $n = 43$  and  $N^+ = 2$  Rydberg-Stark states. On longer timescales, transfer to high- $|m_\ell|$  states through collisions or interactions with time-dependent electric fields after photoexcitation [49], and effects of blackbody-radiation-induced transitions become apparent. Blackbody transitions have an approximately equal probability of increasing or decreasing the values of  $n$  and  $|m_\ell|$ , but preserve the electric dipole moments and

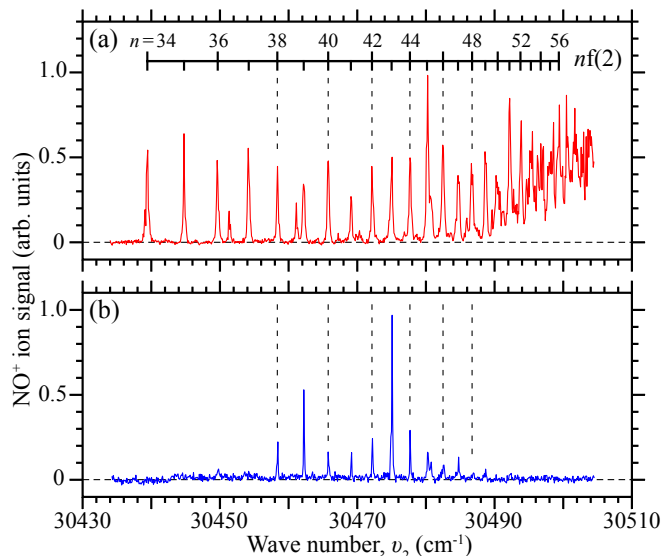


FIG. 4. Laser photoexcitation spectra recorded (a) upon detection by PFI  $\sim 50$  ns after photoexcitation, and (b) after deceleration and trapping for  $20 \mu\text{s}$  with  $V_0 = 125$  V and  $T_{\text{env}} = 30$  K.

LFS character of the molecules, allowing them to remain trapped. However, because lower  $|m_\ell|$  states decay more rapidly, at longer trapping times only molecules in longer-lived higher  $|m_\ell|$  states remain. Consequently, the rate of decay from the trap reduces. For  $T_{\text{env}} = 295$  K the number of trapped molecules was lower than for  $T_{\text{env}} = 30$  K. To allow direct comparison, the data in Figure 3 have been normalized. Those recorded for  $T_{\text{env}} = 295$  K were truncated at  $0.6$  ms where the signal had decayed to the level of the background noise. For  $50 \leq t_{\text{trap}} \leq 350 \mu\text{s}$  the data recorded for  $T_{\text{env}} = 295$  K can be described by a single exponential function with  $\tau = 172 \pm 10 \mu\text{s}$  (dashed red curve). Under these conditions, the decay of the molecules from the trap is affected by blackbody photoionization [33, 46], and slow dissociation following blackbody transitions to states with  $|m_\ell| \lesssim 3$ .

For  $V_0 = 125$  V, molecules in states with values of  $n$  from 38 to 49 could be decelerated and trapped. This Rydberg-state acceptance was determined from the spectra in Figure 4. The spectrum in Figure 4(a) was recorded by PFI  $\sim 50$  ns after photoexcitation and is dominated by transitions to  $nf(2)$  Rydberg states. This is because, for the values of  $n$  studied, the short predissociation times of the  $np(0)$  states ( $< 1$  ns [58]) preclude their detection. The spectrum in Figure 4(b) was obtained by detecting only molecules that were decelerated and trapped for  $20 \mu\text{s}$  at  $T_{\text{env}} = 30$  K. For the lowest (highest) values of  $n$  the trapping efficiency reduces in part because the maximal electric dipole moments (ionization electric fields) reduce and greater losses occur during deceleration. The relative intensities of the individual spec-

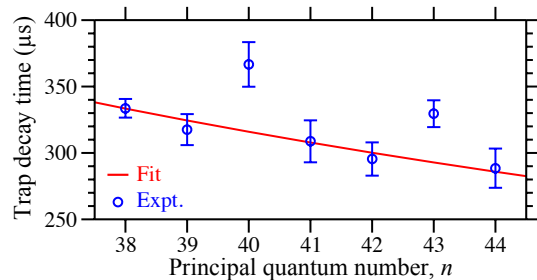


FIG. 5. Rydberg-state dependence of  $\tau$  determined for states with  $N^+ = 2$  and  $50 \leq t_{\text{trap}} \leq 350 \mu\text{s}$  with  $V_0 = 125$  and  $T_{\text{env}} = 30$  K (open blue circles). The continuous red curve for which  $\tau = 15197 n^{-1.05} \mu\text{s}$  was fit to the experimental data for values of  $n$  excluding 40 and 43 (see text for details).

tral features reflect the efficiencies with which long-lived hydrogenic Rydberg-Stark states were populated upon excitation at each resonance, and the contributions from intramolecular interactions that cause slow dissociation during deceleration and trap loading.

The decay of molecules with  $38 \leq n \leq 44$  and  $N^+ = 2$  was measured for  $T_{\text{env}} = 30$  K, and  $\tau$  was determined for  $50 \leq t_{\text{trap}} \leq 350 \mu\text{s}$ . These decay times (blue points in Figure 5 that represent the average of multiple measurements) are shorter than the corresponding fluorescence lifetimes,  $\tau_{\text{fl}}$ , of  $\ell$ -mixed Rydberg-Stark states with  $|m_\ell| = 3$  in the H atom for which  $\tau_{\text{fl}} \propto n^4$  and  $\tau_{\text{fl}}(n = 38) = 547 \mu\text{s}$ . In general, the decay times in Figure 5 reduce as the value of  $n$  increases. The red curve represents the function  $15197 n^{-1.05} \mu\text{s}$  fit to the data for values of  $n$  excluding 40 and 43. This behavior is not representative of the trap decay observed for atomic Rydberg states and is attributed to the gradual increase in the strength of intramolecular interactions of the high- $n$  hydrogenic Rydberg-Stark states in the series with  $N^+ = 2$  and  $v^+ = 0$ , with short-lived states in series converging to other rotational or vibrational states of the  $\text{NO}^+$  ion core as the  $N^+ = 2$  series limit is approached.

The  $n = 40$  and  $43$  states in Figure 5 exhibit trap decay times that do not follow this  $n^{-1}$  scaling. These states are almost degenerate with the hydrogenic Rydberg-Stark states in the  $N^+ = 0$  series for which  $n = 44$  and  $48$ , respectively. Mixing between these near degenerate Stark manifolds, for which  $\Delta N^+ = 2$ , arises as a result of the charge-quadrupole interaction of the Rydberg electron with the  $\text{NO}^+$  ion core [59]. The enhanced trapping times for these values of  $n$  appear to be a consequence of these intramolecular interactions and indicate that the  $n = 44$  and  $48$  states in the  $N^+ = 0$  series exhibit longer lifetimes than the  $n = 40$  and  $43$  states with  $N^+ = 2$ .

In conclusion, we have demonstrated electrostatic trapping of NO molecules in long-lived hydrogenic Rydberg-Stark states. Significant differences in the trap decay times for  $T_{\text{env}} = 295$  and  $30$  K highlight effects



of blackbody photoionization, and slow dissociation following blackbody induced transitions between Rydberg states. Measurements performed for a range of values of  $n$  yielded new insights into effects of intramolecular interactions on slow decay process of long-lived Rydberg states in NO.

This work was supported by the European Research Council (ERC) under the European Union's Horizon 2020 research and innovation program (Grant No. 683341). M. H. R. is grateful to the Engineering and Physical Sciences Research Council for a Vacation Bursary, and support through the Doctoral Training Partnership (Grant No. EP/R513143/1).

---

\* Present address: Max-Planck-Institut für Plasmaphysik, Boltzmannstraße 2, 85748 Garching bei München, Germany.

- [1] N. Hölsch, M. Beyer, E. J. Salumbides, K. S. E. Eikema, W. Ubachs, Ch. Jungen, and F. Merkt, Benchmarking Theory with an Improved Measurement of the Ionization and Dissociation Energies of  $\text{H}_2$ , *Phys. Rev. Lett.* **122**, 103002 (2019)
- [2] R. Peverall, S. Rosén, J. R. Peterson, M. Larsson, A. Al-Khalili, L. Viktor, J. Semaniak, R. Bobbenkamp, A. Le Padellec, A. N. Maurellis and W. J. van der Zande, Dissociative Recombination and Excitation of  $\text{O}_2^+$ : Cross Sections, Product Yields and Implications for Studies of Ionospheric Airglows, *J. Chem. Phys.* **114**, 6679 (2001)
- [3] S. L. Guberman, Role of Excited Core Rydberg States in Dissociative Recombination, *J. Phys. Chem. A* **111**, 11254 (2007)
- [4] J. P. Morrison, C. J. Rennick, J. S. Keller, and E. R. Grant, Evolution from a Molecular Rydberg Gas to an Ultracold Plasma in a Seeded Supersonic Expansion of NO, *Phys. Rev. Lett.* **101**, 205005 (2008)
- [5] H. Sadeghi, A. Kruey, J. Hung, J. H. Gurian, J. P. Morrison, M. Schulz-Weiling, N. Saquet, C. J. Rennick, and E. R. Grant, Dissociation and the Development of Spatial Correlation in a Molecular Ultracold Plasma, *Phys. Rev. Lett.* **112**, 075001 (2014)
- [6] K. A. Smith, F. G. Kellert, R. D. Rundel, F. B. Dunning, and R. F. Stebbings, Discrete Energy Transfer in Collisions of  $\text{Xe}(nf)$  Rydberg Atoms with  $\text{NH}_3$  Molecules, *Phys. Rev. Lett.* **40**, 1362 (1978)
- [7] K. A. Safinya, J. F. Delpech, F. Goumand, W. Sandner, and T. F. Gallagher, Resonant Rydberg-Atom-Rydberg-Atom Collisions, *Phys. Rev. Lett.* **47**, 405 (1981)
- [8] K. Gawlas and S. D. Hogan, Rydberg-State-Resolved Resonant Energy Transfer in Cold Electric-Field-Controlled Intrabeam Collisions of  $\text{NH}_3$  with Rydberg He Atoms, *J. Phys. Chem. Lett.* **11**, 83 (2020)
- [9] C. H. Greene, A. S. Dickinson, and H. R. Sadeghpour, Creation of Polar and Nonpolar Ultra-Long-Range Rydberg Molecules, *Phys. Rev. Lett.* **85**, 2458 (2000)
- [10] V. Bendkowsky, B. Butscher, J. Nipper, J. P. Shaffer, R. Löw, and T. Pfau, Observation of Ultralong-Range Rydberg Molecules, *Nature* **458**, 1005 (2009)
- [11] M. Kelley, S. Buathong, and F. B. Dunning, Very Strong Rydberg Atom Scattering in  $\text{K}(12p)\text{-CH}_3\text{NO}_2$  Collisions: Role of Transient Ion Pair Formation, *J. Chem. Phys.* **146**, 184307 (2017)
- [12] F. Engel, T. Dieterle, F. Hummel, C. Fey, P. Schmelcher, R. Löw, T. Pfau, and F. Meinert, Precision Spectroscopy of Negative-Ion Resonances in Ultralong-Range Rydberg Molecules, *Phys. Rev. Lett.* **123**, 073003 (2019)
- [13] P. Allmendinger, J. Deiglmayr, K. Höveler, O. Schullian, and F. Merkt, Observation of Enhanced Rate Coefficients in the  $\text{H}_2^+ + \text{H}_2 \rightarrow \text{H}_3^+ + \text{H}$  Reaction at Low Collision Energies, *J. Chem. Phys.* **145**, 244316 (2016)
- [14] J. M. Doyle, B. Friedrich, J. Kim, and D. Patterson, Buffer-Gas Loading of Atoms and Molecules into a Magnetic Trap, *Phys. Rev. A* **52**, 2515(R) (1995)
- [15] H. L. Bethlem, G. Berden, and G. Meijer, Decelerating Neutral Dipolar Molecules, *Phys. Rev. Lett.* **83**, 1558 (1999)
- [16] X. Wang, M. Kirste, G. Meijer, and S. Y.T. van de Meerakker, Stark Deceleration of NO Radicals, *Z. für Phys. Chem.* **227**, 1595 (2013)
- [17] N. Vanhaecke, U. Meier, M. Andrist, B. H. Meier, and F. Merkt, Multistage Zeeman Deceleration of Hydrogen Atoms, *Phys. Rev. A* **75**, 031402(R) (2007)
- [18] E. Narevicius, A. Libson, Ch. G. Parthey, I. Chavez, J. Narevicius, U. Even, and M. G. Raizen, Stopping Supersonic Oxygen with a Series of Pulsed Electromagnetic Coils: A Molecular Coilgun, *Phys. Rev. A* **77**, 051401(R) (2008)
- [19] E. S. Shuman, J. F. Barry, D. R. Glenn, and D. DeMille, Radiative Force from Optical Cycling on a Diatomic Molecule, *Phys. Rev. Lett.* **103**, 223001 (2009)
- [20] E. S. Shuman, J. F. Barry, and D. DeMille, Laser Cooling of a Diatomic Molecule, *Nature* **467**, 820 (2010)
- [21] P. Jansen, L. Semeria, and F. Merkt, Determination of the Spin-Rotation Fine Structure of  $\text{He}_2^+$ , *Phys. Rev. Lett.* **120**, 043001 (2018)
- [22] W. H. Wing, Electrostatic Trapping of Neutral Atomic Particles, *Phys. Rev. Lett.* **45**, 631 (1980)
- [23] T. Breeden and H. Metcalf, Stark Acceleration of Rydberg Atoms in Inhomogeneous Electric Fields, *Phys. Rev. Lett.* **47**, 1726 (1981)
- [24] S. D. Hogan, Rydberg-Stark Deceleration of Atoms and Molecules, *EPJ Techniques and Instrumentation* **3**, 2 (2016)
- [25] D. Townsend, A. L. Goodgame, S. R. Procter, S. R. Mackenzie, and T. P. Softley, Deflection of Krypton Rydberg Atoms in the Field of an Electric Dipole, *J. Phys. B: At. Mol. Opt. Phys.* **34**, 439 (2001)
- [26] Y. Yamakita, S. R. Procter, A. L. Goodgame, and T. P. Softley, and F. Merkt, Deflection and Deceleration of Hydrogen Rydberg Molecules in Inhomogeneous Electric Fields, *J. Chem. Phys.* **121**, 1419 (2004)
- [27] E. Vliegen, H. J. Wörner, T. P. Softley, and F. Merkt, Nonhydrogenic Effects in the Deceleration of Rydberg Atoms in Inhomogeneous Electric Fields, *Phys. Rev. Lett.* **92**, 033005 (2004)
- [28] E. Vliegen and F. Merkt, On the Electrostatic Deceleration of Argon Atoms in High Rydberg States by Time-Dependent Inhomogeneous Electric Fields, *J. Phys. B: At. Mol. Opt. Phys.* **38**, 1623 (2005)
- [29] P. Lancuba and S. D. Hogan, Guiding Rydberg Atoms above Surface-Based Transmission Lines, *Phys. Rev. A* **88**, 043427 (2013)
- [30] P. Allmendinger, J. Deiglmayr, J. A. Agner, H. Schmutz, and F. Merkt, Surface-Electrode Decelerator and Deflec-

- tor for Rydberg Atoms and Molecules, *Phys. Rev. A* **90**, 043403 (2014)
- [31] H. Ko and S. D. Hogan, High-Field-Seeking Rydberg Atoms Orbiting a Charged Wire, *Phys. Rev. A* **89**, 053410 (2014)
- [32] A. Deller, A. M. Alonso, B. S. Cooper, S. D. Hogan, and D. B. Cassidy, Electrostatically Guided Rydberg Positronium, *Phys. Rev. Lett.* **117**, 073202 (2016)
- [33] A. Deller and S. D. Hogan, Confinement of High- and Low-Field-Seeking Rydberg Atoms Using Time-Varying Inhomogeneous Electric Fields, *Phys. Rev. Lett.* **122**, 053203 (2019)
- [34] A. M. Alonso, B. S. Cooper, A. Deller, L. Gurung, S. D. Hogan, and D. B. Cassidy, Velocity Selection of Rydberg Positronium using a Curved Electrostatic Guide, *Phys. Rev. A* **95**, 053409 (2017)
- [35] E. Vliegen, P. A. Limacher, and F. Merkt, Measurement of the three-dimensional velocity distribution of Stark-decelerated Rydberg atoms, *Eur. Phys. J. D*, **40**, 73 (2006)
- [36] E. Vliegen and F. Merkt, Normal-Incidence Electrostatic Rydberg Atom Mirror, *Phys. Rev. Lett.* **97**, 033002 (2006)
- [37] A. C. L. Jones, J. Moxom, H. J. Rutbeck-Goldman, K. A. Osorno, G. G. Cecchini, M. Fuentes-Garcia, R. G. Greaves, D. J. Adams, H. W. K. Tom, A. P. Mills, Jr., and M. Leventhal, Focusing of a Rydberg Positronium Beam with an Ellipsoidal Electrostatic Mirror, *Phys. Rev. Lett.* **119**, 053201 (2017)
- [38] J. Palmer and S. D. Hogan, Experimental Demonstration of a Rydberg-Atom Beam Splitter, *Phys. Rev. A* **95**, 053413 (2017)
- [39] E. Vliegen and F. Merkt, Stark Deceleration of Hydrogen atoms, *J. Phys. B: At. Mol. Opt. Phys.* **39**, L241 (2006)
- [40] S. D. Hogan, P. Allmendinger, H. Saßmannshausen, H. Schmutz, and F. Merkt, Surface-Electrode Rydberg-Stark Decelerator, *Phys. Rev. Lett.* **108**, 063008 (2012)
- [41] P. Lancuba and S. D. Hogan, Transmission-Line Decelerators for Atoms in High Rydberg States, *Phys. Rev. A* **90**, 053420 (2014)
- [42] E. Vliegen, S. D. Hogan, H. Schmutz, and F. Merkt, Stark Deceleration and Trapping of Hydrogen Rydberg Atoms, *Phys. Rev. A* **76**, 023405 (2007)
- [43] S. D. Hogan and F. Merkt, Demonstration of Three-Dimensional Electrostatic Trapping of State-Selected Rydberg Atoms, *Phys. Rev. Lett.* **100**, 043001 (2008)
- [44] S. D. Hogan, Ch. Seiler, and F. Merkt, Rydberg-State-Enabled Deceleration and Trapping of Cold Molecules, *Phys. Rev. Lett.* **103**, 123001 (2009)
- [45] P. Lancuba and S. D. Hogan, Electrostatic Trapping and *in situ* Detection of Rydberg Atoms above Chip-Based Transmission Lines, *J. Phys. B: At. Mol. Opt. Phys.* **49**, 074006 (2016)
- [46] Ch. Seiler, S. D. Hogan, H. Schmutz, J. A. Agner, and F. Merkt, Collisional and Radiative Processes in Adiabatic Deceleration, Deflection, and Off-Axis Trapping of a Rydberg Atom Beam, *Phys. Rev. Lett.* **106**, 073003 (2011)
- [47] S. D. Hogan, Ch. Seiler, and F. Merkt, Motional, Isotope and Quadratic Stark Effects in Rydberg-Stark Deceleration and Electric Trapping of H and D, *J. Phys. B: At. Mol. Opt. Phys.* **46**, 045303 (2013)
- [48] Ch. Seiler, Rydberg-Stark Deceleration and Trapping of Atoms and Molecules, PhD Thesis, ETH Zurich (2013)
- [49] Ch. Seiler, J. A. Agner, P. Pillet, and F. Merkt, Radiative and Collisional Processes in Translationally Cold Samples of Hydrogen Rydberg Atoms Studied in an Electrostatic Trap, *J. Phys. B: At. Mol. Opt. Phys.* **49**, 094006 (2016)
- [50] V. Zhelyazkova, M. Žeško, H. Schmutz, J. A. Agner, and F. Merkt, Fluorescence-Lifetime-Limited Trapping of Rydberg Helium Atoms on a Chip, **117**, 2980 (2019)
- [51] D. B. Cassidy, Experimental Progress in Positronium Laser Physics, *Eur. Phys. J. D* **72**, 53 (2018)
- [52] J. E. Palmer and S. D. Hogan, Electric Rydberg-Atom Interferometry, *Phys. Rev. Lett.* **122**, 250404 (2019)
- [53] M. Seaver, W. A. Chupka, S. D. Colson, and D. Gauyacq, Double Resonance Multiphoton Ionization Studies of High Rydberg States in Nitric Oxide (NO), *J. Phys. Chem.* **87**, 2226 (1983)
- [54] T. Ebata, Y. Anezaki, M. Fujii, N. Mikami, and M. Ito, High Rydberg States of Nitric Oxide Studied by Two-Color Multiphoton Spectroscopy, *J. Phys. Chem.* **87**, 4773 (1983)
- [55] R. Patel, N. J. A. Jones, and H. H. Fielding, Observation of the Stark Effect in  $v^+ = 0$  Rydberg States of NO with a Matrix-Diagonalization Analysis, *J. Phys. B: At. Mol. Opt. Phys.* **40**, 1369 (2007)
- [56] A. Deller and S. D. Hogan, Excitation and Characterization of Long-Lived Hydrogenic Rydberg States of Nitric Oxide, *J. Chem. Phys.* **152**, 144305 (2020)
- [57] J. Schmidt, M. Fiedler, R. Albrecht, D. Djekic, P. Schallberger, H. Baur, R. Löw, N. Fruehauf, T. Pfau, J. Anders, E. R. Grant, and H. Kübler, Proof of Concept for an Optogalvanic Gas Sensor for NO Based on Rydberg Excitations, *Appl. Phys. Lett.* **113**, 011113 (2018)
- [58] M. J. J. Vrakking and Y. T. Lee, Lifetimes of Rydberg States in Zero-Electron-Kinetic-Energy Experiments. I. Electric Field Induced and Collisional Enhancement of NO Predissociation Lifetimes, *J. Chem. Phys.* **102**, 8818 (1995)
- [59] M. Bixon and J. Jortner, Intramolecular Coupling between Non-Penetrating High Molecular Rydberg States, *Mol. Phys.*, **89**, 373 (1996)